Biomedical Optics EXPRESS

Microstructure of subretinal drusenoid deposits revealed by adaptive optics imaging

Alexander Meadway,[1] Xiaolin Wang,[1] Christine A. Curcio,[1] and Yuhua Zhang[1,2,3,*]

[1]*Department of Ophthalmology, University of Alabama at Birmingham, 1670 University Boulevard, Birmingham, Al 35294, USA*

[2]*Department of Vision Sciences, University of Alabama at Birmingham, 1530 3rd Avenue South, Birmingham, AL 35294, USA*

[3]*Department of Biomedical Engineering, University of Alabama at Birmingham, 1825 University Boulevard, Birmingham, AL 35294, USA*

**zhanghua@uab.edu*

Abstract: Subretinal drusenoid deposits (SDD), a recently recognized lesion associated with progression of age-related macular degeneration, were imaged with adaptive optics scanning laser ophthalmoscopy (AO-SLO) and optical coherence tomography (AO-OCT). AO-SLO revealed a distinct *en face* structure of stage 3 SDD, showing a hyporeflective annulus surrounded reflective core packed with hyperreflective dots bearing a superficial similarity to the photoreceptors in the unaffected retina. However, AO-OCT suggested that the speckled appearance over the SDD rendered by AO-SLO was the lesion material itself, rather than photoreceptors. AO-OCT assists proper interpretation and understanding of the SDD structure and the lesions' impact on surrounding photoreceptors produced by AO-SLO and vice versa.

OCIS codes: (110.1080) Active or adaptive optics; (110.4500) Optical coherence tomography; (330.5310) Vision - photoreceptors; (330.7329) Visual optics, pathology.

References and links

1. M. Rudolf, G. Malek, J. D. Messinger, M. E. Clark, L. Wang, and C. A. Curcio, "Sub-retinal drusenoid deposits in human retina: organization and composition," Exp. Eye Res. **87**(5), 402–408 (2008).
2. C. A. Curcio, J. D. Messinger, K. R. Sloan, G. McGwin, N. E. Medeiros, and R. F. Spaide, "Subretinal drusenoid deposits in non-neovascular age-related macular degeneration: morphology, prevalence, topography, and biogenesis model," Retina **33**(2), 265–276 (2013).
3. G. Mimoun, G. Soubrane, and G. Coscas, "[Macular drusen]," J. Fr. Ophtalmol. **13**(10), 511–530 (1990).
4. J. Sarks, J. Arnold, I. V. Ho, S. Sarks, and M. Killingsworth, "Evolution of reticular pseudodrusen," Br. J. Ophthalmol. **95**(7), 979–985 (2011).
5. S. Y. Cohen, L. Dubois, R. Tadayoni, C. Delahaye-Mazza, C. Debibie, and G. Quentel, "Prevalence of reticular pseudodrusen in age-related macular degeneration with newly diagnosed choroidal neovascularisation," Br. J. Ophthalmol. **91**(3), 354–359 (2007).
6. S. Schmitz-Valckenberg, F. Alten, J. S. Steinberg, G. J. Jaffe, M. Fleckenstein, B. N. Mukesh, T. C. Hohman, and F. G. Holz; Geographic Atrophy Progression (GAP) Study Group, "Reticular drusen associated with geographic atrophy in age-related macular degeneration," Invest. Ophthalmol. Vis. Sci. **52**(9), 5009–5015 (2011).
7. L. Xu, A. M. Blonska, N. M. Pumariega, S. Bearelly, M. A. Sohrab, G. S. Hageman, and R. T. Smith, "Reticular macular disease is associated with multilobular geographic atrophy in age-related macular degeneration," Retina **33**(9), 1850–1862 (2013).
8. M. Marsiglia, S. Boddu, S. Bearelly, L. Xu, B. E. Breaux, Jr., K. B. Freund, L. A. Yannuzzi, and R. T. Smith, "Association between geographic atrophy progression and reticular pseudodrusen in eyes with dry age-related macular degeneration," Invest. Ophthalmol. Vis. Sci. **54**(12), 7362–7369 (2013).
9. R. F. Spaide, "Outer retinal atrophy after regression of subretinal drusenoid deposits as a newly recognized form of late age-related macular degeneration," Retina **33**(9), 1800–1808 (2013).
10. S. A. Zweifel, R. F. Spaide, C. A. Curcio, G. Malek, and Y. Imamura, "Reticular pseudodrusen are subretinal drusenoid deposits," Ophthalmology **117**(2), 303–312 (2010).
11. S. Schmitz-Valckenberg, J. S. Steinberg, M. Fleckenstein, S. Visvalingam, C. K. Brinkmann, and F. G. Holz, "Combined confocal scanning laser ophthalmoscopy and spectral-domain optical coherence tomography

#201230 - $15.00 USD Received 14 Nov 2013; revised 18 Jan 2014; accepted 5 Feb 2014; published 12 Feb 2014

imaging of reticular drusen associated with age-related macular degeneration," Ophthalmology **117**(6), 1169–1176 (2010).
12. G. Querques, M. Srour, N. Massamba, N. Puche, and E. H. Souied, "Reticular pseudodrusen," Ophthalmology **120**(4), 872 (2013).
13. G. Querques, L. Querques, D. Martinelli, N. Massamba, G. Coscas, G. Soubrane, and E. H. Souied, "Pathologic insights from integrated imaging of reticular pseudodrusen in age-related macular degeneration," Retina **31**(3), 518–526 (2011).
14. G. Querques, F. Canouï-Poitrine, F. Coscas, N. Massamba, L. Querques, G. Mimoun, F. Bandello, and E. H. Souied, "Analysis of progression of reticular pseudodrusen by spectral domain-optical coherence tomography," Invest. Ophthalmol. Vis. Sci. **53**(3), 1264–1270 (2012).
15. J. Liang, D. R. Williams, and D. T. Miller, "Supernormal vision and high-resolution retinal imaging through adaptive optics," J. Opt. Soc. Am. A **14**(11), 2884–2892 (1997).
16. A. Roorda, F. Romero-Borja, W. Donnelly III, H. Queener, T. Hebert, and M. Campbell, "Adaptive optics scanning laser ophthalmoscopy," Opt. Express **10**(9), 405–412 (2002).
17. R. J. Zawadzki, S. M. Jones, S. S. Olivier, M. Zhao, B. A. Bower, J. A. Izatt, S. Choi, S. Laut, and J. S. Werner, "Adaptive-optics optical coherence tomography for high-resolution and high-speed 3D retinal in vivo imaging," Opt. Express **13**(21), 8532–8546 (2005).
18. Y. Zhang, S. Poonja, and A. Roorda, "MEMS-based adaptive optics scanning laser ophthalmoscopy," Opt. Lett. **31**(9), 1268–1270 (2006).
19. Y. Zhang, S. Poonja, and A. Roorda, "AOSLO: from benchtop to clinic," Proc. SPIE **6306**, 63060V (2006).
20. Y. Zhang, B. Cense, J. Rha, R. S. Jonnal, W. Gao, R. J. Zawadzki, J. S. Werner, S. Jones, S. Olivier, and D. T. Miller, "High-speed volumetric imaging of cone photoreceptors with adaptive optics spectral-domain optical coherence tomography," Opt. Express **14**(10), 4380–4394 (2006).
21. S. A. Burns, R. Tumbar, A. E. Elsner, D. Ferguson, and D. X. Hammer, "Large-field-of-view, modular, stabilized, adaptive-optics-based scanning laser ophthalmoscope," J. Opt. Soc. Am. A **24**(5), 1313–1326 (2007).
22. R. J. Zawadzki, S. S. Choi, S. M. Jones, S. S. Oliver, and J. S. Werner, "Adaptive optics-optical coherence tomography: optimizing visualization of microscopic retinal structures in three dimensions," J. Opt. Soc. Am. A **24**(5), 1373–1383 (2007).
23. R. J. Zawadzki, B. Cense, Y. Zhang, S. S. Choi, D. T. Miller, and J. S. Werner, "Ultrahigh-resolution optical coherence tomography with monochromatic and chromatic aberration correction," Opt. Express **16**(11), 8126–8143 (2008).
24. A. Roorda, "Applications of adaptive optics scanning laser ophthalmoscopy," Optom. Vis. Sci. **87**(4), 260–268 (2010).
25. D. T. Miller, O. P. Kocaoglu, Q. Wang, and S. Lee, "Adaptive optics and the eye (super resolution OCT)," Eye (Lond.) **25**(3), 321–330 (2011).
26. A. Dubra, Y. Sulai, J. L. Norris, R. F. Cooper, A. M. Dubis, D. R. Williams, and J. Carroll, "Noninvasive imaging of the human rod photoreceptor mosaic using a confocal adaptive optics scanning ophthalmoscope," Biomed. Opt. Express **2**(7), 1864–1876 (2011).
27. R. J. Zawadzki, S. M. Jones, S. Pilli, S. Balderas-Mata, D. Y. Kim, S. S. Olivier, and J. S. Werner, "Integrated adaptive optics optical coherence tomography and adaptive optics scanning laser ophthalmoscope system for simultaneous cellular resolution in vivo retinal imaging," Biomed. Opt. Express **2**(6), 1674–1686 (2011).
28. D. X. Hammer, R. D. Ferguson, M. Mujat, A. Patel, E. Plumb, N. Iftimia, T. Y. Chui, J. D. Akula, and A. B. Fulton, "Multimodal adaptive optics retinal imager: design and performance," J. Opt. Soc. Am. A **29**(12), 2598–2607 (2012).
29. S. Mrejen, T. Sato, C. A. Curcio, and R. F. Spaide, "Assessing the Cone Photoreceptor Mosaic in Eyes with Pseudodrusen and Soft Drusen In Vivo Using Adaptive Optics Imaging," Ophthalmology **121**(2), 545–551 (2013).
30. Y. Zhang, X. Wang, E. R. Blanco, M. E. Clark, C. D. Witherspoon, R. F. Spaide, C. A. Girkin, C. Owsley, and C. A. Curcio, "Photoreceptor perturbation around subretinal drusenoid deposits revealed by adaptive optics scanning laser ophthalmoscopy," Am. J. Ophthalmol. (In review).
31. R. F. Spaide, "Questioning optical coherence tomography," Ophthalmology **119**(11), 2203–2204 (2012).
32. R. F. Spaide and C. A. Curcio, "Anatomical correlates to the bands seen in the outer retina by optical coherence tomography: literature review and model," Retina **31**(8), 1609–1619 (2011).
33. A. Meadway, C. A. Girkin, and Y. Zhang, "A dual-modal retinal imaging system with adaptive optics," Opt. Express **21**(24), 29792–29807 (2013).
34. Y. Zhang, J. Rha, R. Jonnal, and D. Miller, "Adaptive optics parallel spectral domain optical coherence tomography for imaging the living retina," Opt. Express **13**(12), 4792–4811 (2005).
35. F. C. Delori, R. H. Webb, and D. H. Sliney; American National Standards Institute, "Maximum permissible exposures for ocular safety (ANSI 2000), with emphasis on ophthalmic devices," J. Opt. Soc. Am. A **24**(5), 1250–1265 (2007).
36. C. R. Vogel, D. W. Arathorn, A. Roorda, and A. Parker, "Retinal motion estimation in adaptive optics scanning laser ophthalmoscopy," Opt. Express **14**(2), 487–497 (2006).
37. R. F. Spaide and C. A. Curcio, "Drusen characterization with multimodal imaging," Retina **30**(9), 1441–1454 (2010).

#201230 - $15.00 USD Received 14 Nov 2013; revised 18 Jan 2014; accepted 5 Feb 2014; published 12 Feb 2014

38. N. Ueda-Arakawa, S. Ooto, A. Tsujikawa, K. Yamashiro, A. Oishi, and N. Yoshimura, "Sensitivity and specificity of detecting reticular pseudodrusen in multimodal imaging in Japanese patients," Retina **33**(3), 490–497 (2013).
39. A. Pallikaris, D. R. Williams, and H. Hofer, "The reflectance of single cones in the living human eye," Invest. Ophthalmol. Vis. Sci. **44**(10), 4580–4592 (2003).
40. R. F. Cooper, A. M. Dubis, A. Pavaskar, J. Rha, A. Dubra, and J. Carroll, "Spatial and temporal variation of rod photoreceptor reflectance in the human retina," Biomed. Opt. Express **2**(9), 2577–2589 (2011).
41. O. P. Kocaoglu, S. Lee, R. S. Jonnal, Q. Wang, A. E. Herde, J. C. Derby, W. Gao, and D. T. Miller, "Imaging cone photoreceptors in three dimensions and in time using ultrahigh resolution optical coherence tomography with adaptive optics," Biomed. Opt. Express **2**(4), 748–763 (2011).
42. M. A. Sohrab, R. T. Smith, H. Salehi-Had, S. R. Sadda, and A. A. Fawzi, "Image registration and multimodal imaging of reticular pseudodrusen," Invest. Ophthalmol. Vis. Sci. **52**(8), 5743–5748 (2011).
43. Y. Zhang, S. Poonja, and A. Roorda, "Adaptive optics scanning laser ophthalmoscope using a micro-electro-mechanical (MEMS) deformable mirror," Proc. SPIE **6138**, 61380Z (2006).
44. C. A. Curcio, J. B. Presley, C. L. Millican, and N. E. Medeiros, "Basal deposits and drusen in eyes with age-related maculopathy: evidence for solid lipid particles," Exp. Eye Res. **80**(6), 761–775 (2005).
45. J. D. Huang, J. B. Presley, M. F. Chimento, C. A. Curcio, and M. Johnson, "Age-related changes in human macular Bruch's membrane as seen by quick-freeze/deep-etch," Exp. Eye Res. **85**(2), 202–218 (2007).
46. C. A. Curcio, M. Johnson, J.-D. Huang, and M. Rudolf, "Aging, age-related macular degeneration, and the Response-to-Retention of apolipoprotein B-containing lipoproteins," Prog. Retin. Eye Res. **28**(6), 393–422 (2009).
47. R. F. Mullins, L. V. Johnson, D. H. Anderson, and G. S. Hageman, "Characterization of drusen-associated glycoconjugates," Ophthalmology **104**(2), 288–294 (1997).
48. C. M. Li, M. E. Clark, M. Rudolf, and C. A. Curcio, "Distribution and composition of esterified and unesterified cholesterol in extra-macular drusen," Exp. Eye Res. **85**(2), 192–201 (2007).
49. V. Luibl, J. M. Isas, R. Kayed, C. G. Glabe, R. Langen, and J. Chen, "Drusen deposits associated with aging and age-related macular degeneration contain nonfibrillar amyloid oligomers," J. Clin. Invest. **116**(2), 378–385 (2006).
50. S. H. Sarks, D. Van Driel, L. Maxwell, and M. Killingsworth, "Softening of drusen and subretinal neovascularization," Trans. Ophthalmol. Soc. U. K. **100**(3), 414–422 (1980).

1. Introduction

Subretinal drusenoid deposits (SDD) [1] are extracellular lesions recently recognized in eyes with age-related macular degeneration (AMD) [2]. These space-filling lesions are found between the photoreceptors and their supporting retinal pigment epithelium (RPE) cell layer, in a compartment called subretinal space inside the physiological blood-retina barrier [1, 2]. Histopathologic studies suggest that SDD clinically manifest as pseudodrusen [2–4], biomicroscopic signs visible in multiple imaging modalities that are highly associated with progression to choroidal neovascularization (CNV), geographic atrophy (GA) [5–8], and outer retinal atrophy [9]. The subretinal location of pseudodrusen was revealed and consolidated by spectral domain optical coherence tomography (SD-OCT) [10–14]. A 3-stage OCT based grading system has been introduced to classify the development of SDD [10].

Because of their proximity to the overlying photoreceptors, SDD may impose a more direct impact on the optical properties and structure of the photoreceptors. Histology indicates that SDD are associated with significant photoreceptor degeneration, including deflected, shortened, and missing inner and outer segments, as well as reduced number of nuclei in the outer nuclear layer (ONL) [1, 2]. However, these changes are not readily observed by standard clinical imaging modalities due to imaging resolution being limited by low numerical aperture of the imaging system (using small beam size) and the optical defects of the human eye. Recent advances in adaptive optics (AO) retinal imaging [15–28] make it possible to directly assess the impact of SDD on photoreceptors in the living patient eye. A recent study using AO flood illumination fundus camera reported significant photoreceptor loss over stage 3, an advanced stage at which SDD have caused significant disruption of the overlying photoreceptor layer [10], by counting indistinct reflective spots over these lesions [29]. In a study we conducted with adaptive optics scanning laser ophthalmoscope (AO-SLO), we found that stage 3 SDD appeared as a distinct hyporeflective annulus surrounding a reflective core [30] (see results section). The most dramatic feature of these AO-SLO images (of stage 3 SDD) is that the textures of the central cores bear a superficial resemblance to that

#201230 - $15.00 USD Received 14 Nov 2013; revised 18 Jan 2014; accepted 5 Feb 2014; published 12 Feb 2014

of photoreceptors rendered by AO assisted retinal imaging, i.e., regularly spaced reflective spots packed with a mosaic pattern. This raises a question; can this distinctive appearance be attributed to the photoreceptors overlaying the SDD? From our understanding of how AO-SLO images are formed and by examination of cross-sectional images provided by SD-OCT, we deduced that this reflective core consisted of SDD material itself, not photoreceptors [30].

To further understand AO-SLO images of SDD and surrounding photoreceptor cells, we have extended an AO-SLO system with AO-OCT imaging function. With the inherent fine axial resolution of OCT and AO improved lateral resolution [25], the AO-SLO-OCT reveals detailed structure of the retina and improves our understanding of origins of reflections that form AO-SLO image. The AO facilitated *en face* and cross-sectional high-resolution imaging not only provides the microstructure of SDD but also reveals the lesion's impact on surrounding photoreceptors.

2. Methods

2.1 Nomenclature

The nomenclature for subretinal lesions in AMD has varied depending on instrumentation, investigators, and patient population, with SDD used for cross-sectional histology and OCT and reticular pseudodrusen, pseudoreticular drusen, or pseudodrusen for different *en face* modalities [2]. Increasing evidence indicates that many SDD are not reticular (networked) and none are pseudo (false) [12]. In this paper, we will use the term SDD to simplify presentation of AO-SLO-OCT images. We also note the debate over the naming of outer retinal hyper-reflective bands in OCT images [31]. We adopted the nomenclature proposed by Spaide and Curcio [32], which has been used in the OCT based 3-stage SDD grading system [10]. Briefly, for the 4 hyper-reflective outer retinal bands of SD-OCT: (1) a thin band corresponding to the external limiting membrane (ELM); (2) a thick and highly reflective band corresponding to the ellipsoid portion of photoreceptor inner segments (EZ); this band is often called the junction between the inner and outer segment of photoreceptor (IS/OS); (3) a thick but less reflective band corresponding to an ensheathment of cone outer segments by RPE apical processes (interdigitation zone, IZ); most reliably visible outside the central fovea, and (4) a thick and highly reflective band corresponding to the RPE–Bruch's membrane complex.

2.2 AO-SLO-OCT system

The system has been reported elsewhere [33]. The unique feature of this instrument compared to previously reported AO imaging systems [16–18, 20–22, 25–28, 34] is that it is a dual-modal system, including both AO-SLO and AO-OCT. The two imaging modalities use the same light source and share the same light path through the sample and detector arms. Thus, optimal AO compensation for ocular aberration can be achieved in both imaging modes, and images acquired in the two modes can be evaluated without ambiguity induced by different light sources. The light source for both AO-SLO and AO-OCT imaging is a superluminescent diode (SLD) (Broadlighter S840-HP, Superlum, Russia). Its wavelength centres at 840 nm with a bandwidth of 50 nm (FWHM). The light source for wavefront detection is a diode laser with wavelength at 680 nm. The light is delivered to the eye through the scanning optics and adaptive optics and forms a scanning raster on the retina. The pupil size of the instrument is set at 5.6 mm in diameter. The adaptive optics consists of a deformable mirror (Hi-Speed DM97-15, ALPAO SAS, France) and a custom wavefront sensor (WS). The WS is made up of a high speed CMOS camera (MicroVista®-NIR, Intevac Inc., USA) whose spectral response is optimised for near infrared light. A lenslet array of 0.3 mm x 0.3 mm pitch and 7.6 mm focal length (0300-7.6-S, Adaptive Optics Associates, Cambridge, MA) samples the wavefront in 193 sub-apertures with the 512 x 512 pixel sensor. The AO can reduce the root-

#201230 - $15.00 USD Received 14 Nov 2013; revised 18 Jan 2014; accepted 5 Feb 2014; published 12 Feb 2014

mean-square wave aberration to less than 50 nm in most eyes, meeting the Maréchal criterion for diffraction-limited resolution for the wavelength used in imaging.

The AO-SLO imaging channel consists of a photomultiplier tube (PMT) (H7422-50, Hamamatsu, Japan) and custom signal processing electronics controlling the scanning system and forming the output of the PMT to a pseudo-video signal for imaging.

The AO-OCT was implemented with a free space Michelson interferometer scheme by adding a reference arm to the AO-SLO scanning optics. The light from the reference arm combines the light reflected from the human eye forming the interference signal, which is detected by a spectrometer comprising an 1800 lines/mm transmissive diffraction grating and a line scan camera (spL2048-140km, Basler, Germany). Currently only the slow galvo-scanner is used in AO-OCT mode because the resonant scanner of the AO-SLO is too fast for OCT imaging. Thus, it is not possible to collect volume images with the AO-OCT. For each frame 512 lines are collected. Images can be acquired at frame rates up to 140 Hz. The axial resolution of the AO-OCT is measured to be 4.7 μm in the retina.

This instrument is not a system for simultaneous AO-SLO and AO-OCT imaging [27, 28]. The two imaging modes are switched by a flip mirror and an associated beam trap that can allow or absorb the light from the reference arm to enter the detection channel.

2.3 Imaging protocol

The study followed the tenets of the Declaration of Helsinki and was approved by the Institutional Review Board for Human Use (IRB) at the University of Alabama at Birmingham. Written informed consent was obtained from the participants after the nature and possible consequences of the study were explained.

Study patients with AMD and age-similar subjects with normal retinas were recruited from the clinical research registry of the Department of Ophthalmology of the University of Alabama at Birmingham and through the Retina Service. Exclusion criteria included diabetes, history of retinal vascular occlusions, and any signs or history of hereditary retinal dystrophy. Subjects were also excluded for reasons that might potentially prevent successful imaging, such as poor fixation, significant media opacity, irregular pupil shape, poor dilation, or refractive errors greater than ± 6 D spherical and ± 3 D cylinder. The inclusion criteria for normal comparison subjects were the same, with the additional criteria of age greater than 50 years, no clinically significant cataract, and best-corrected visual acuity of 20/25 or better.

Before imaging, the pupil of the subject was dilated using 1.0% tropicamide and 2.5% phenylephrine hydrochloride. The subject's head was aligned and stabilised with the use of a head mount with a chinrest. A fixation target consisting of a blue light dot moving on a calibrated grid was placed in front of the eye via a pellicle beam splitter to help the subject's fixation. The power incident on the cornea in both imaging modes is 0.5 mW, well below the maximum permissible exposure level of the ANSI standards [35]. The AO-SLO field of view was 1°, and the image was digitized with 512 X 512 pixels. The AO-SLO continuously recorded the video so that a 20° field of view retinal image montage can be made. SDD positions were marked on the fixation grid for AO-OCT. AO-OCT B-scans were acquired across a field of view of 1° within less than 60 seconds.

In addition to high resolution AO imaging, colour digital fundus photographs were taken with a FF450 Plus fundus camera (Carl Zeiss Meditec, Dublin, CA), *en face* near infrared (IR) (λ = 830 nm), red-free (RF) (λ = 560 nm), and autofluorescence (AF) (excitation, 488 nm; emission, > 600 nm) images were acquired with a standard confocal SLO (Spectralis, Heidelberg Engineering, Carlsbad, CA). Retinal cross-sections were imaged with SD-OCT of the Spectalis (λ = 870 nm; acquisition speed, 40,000 A-scans per seconds; scan depth, 1.8mm; digital depth resolution, approximately 3.5 μm per pixel). In each study eye, 97 B-scans were acquired across a 15° × 10° area of the central macula to create a volume.

#201230 - $15.00 USD Received 14 Nov 2013; revised 18 Jan 2014; accepted 5 Feb 2014; published 12 Feb 2014

2.4 Image processing

For AO-SLO, image distortion caused by nonlinear scanning of the resonant scanner and by eye movements was eliminated by customized software [36]. Registered images (typically 10-30 frames) were averaged to enhance signal-to-noise ratio. Then, images taken at different retinal locations were aligned with image processing software (Photoshop, Adobe Systems Inc, Mountain View, CA) to create a continuous montage.

AO-OCT images were registered using the StackReg plugin (see acknowledgment) for ImageJ (version 1.47g; http://rsbweb.nih.gov/ij/; National Institutes of Health, Bethesda, MD). When a stable group was found, frames were averaged to produce a single image. Typically sets of 7-10 suitable frames were averaged for imaging at a frame rate of 100 Hz.

Color fundus photographs and IR, RF, AF images taken with the Spectralis SLO were readily registered manually. Color fundus photographs were then magnified and registered with the AO-SLO image montage by use of retinal vessels and capillaries as invariant landmarks. Then SDD apparent on standard funduscopy were localized in AO-SLO images.

2.5 SDD identification and grading

The identification of SDD was based on their presence in multimodal imaging as described previously [4, 10–13, 37, 38]. Briefly, SDD appear as an interlacing collection of ribbons or a dot-like pattern of yellow-white lesions in a color fundus photograph, a pattern of hyporeflective or hyperreflective spots in an IR image, or a pattern of small hypofluorescent areas against a background of mild hyperfluorescence in an AF image. The structures of SDD as well as the RPE were evaluated with SD-OCT volume. They appear as hyperreflective mounds internal to the RPE. The lesions were first identified by their corresponding locations in the registered multimodal images in the *en face* plane, and then examined in the cross-section plane by the SD-OCT. SDD was scored with the 3-stage grading system introduced by Zweifel et al [10]. Stage 1 was defined as diffuse deposition of granular hyperreflective material between the RPE-Bruch's membrane band and the EZ(IS/OS). In stage 2, SDD mounds altered the EZ(IS/OS) band contour. In stage 3, SDD have broken through the EZ(IS/OS). Specific SDD formations and surrounding photoreceptors were examined en face by AO-SLO and exactly the corresponding AO-OCT.

3. Results

3.1 Imaging of healthy retinas

As a reference for the diseased retina, Fig. 1 presents retinal images taken from a subject with healthy retina. AO-SLO reveals a clear photoreceptor mosaic, Fig. 1(b). While individual photoreceptors manifest varying brightness [39, 40], the overall brightness is similar across clusters of adjacent photoreceptors. SD-OCT reveals even and well-aligned outer retinal hyperreflective bands, Fig. 1(c). However, without AO compensation for the ocular aberration, SD-OCT cannot resolve individual photoreceptors EZ(IS/OS).

Shown in Fig. 2 are healthy retinal images of another subject taken with the dual-modal AO-SLO-OCT, approximately 2° nasal to the fovea centre. As familiar from the literature [17, 20, 27, 41], AO-OCT resolves the EZ(IS/OS) of individual photoreceptors. AO correction for ocular aberrations also reduces the depth of focus, and the instrument is adjusted to focus on the photoreceptors. Thus, while all major retinal layers are visible in the OCT image, the photoreceptor-RPE complex is significantly brighter than the inner retinal layers. Note here the AO-OCT image is in linear grey scale. By using a logarithmic grey scale, the inner retinal structure may be more clearly rendered. An important feature to note here is the even and well-aligned outer retinal hyperreflective bands without discernible hyperreflective material between the IZ-RPE and the EZ (IS/OS) bands.

#201230 - $15.00 USD Received 14 Nov 2013; revised 18 Jan 2014; accepted 5 Feb 2014; published 12 Feb 2014

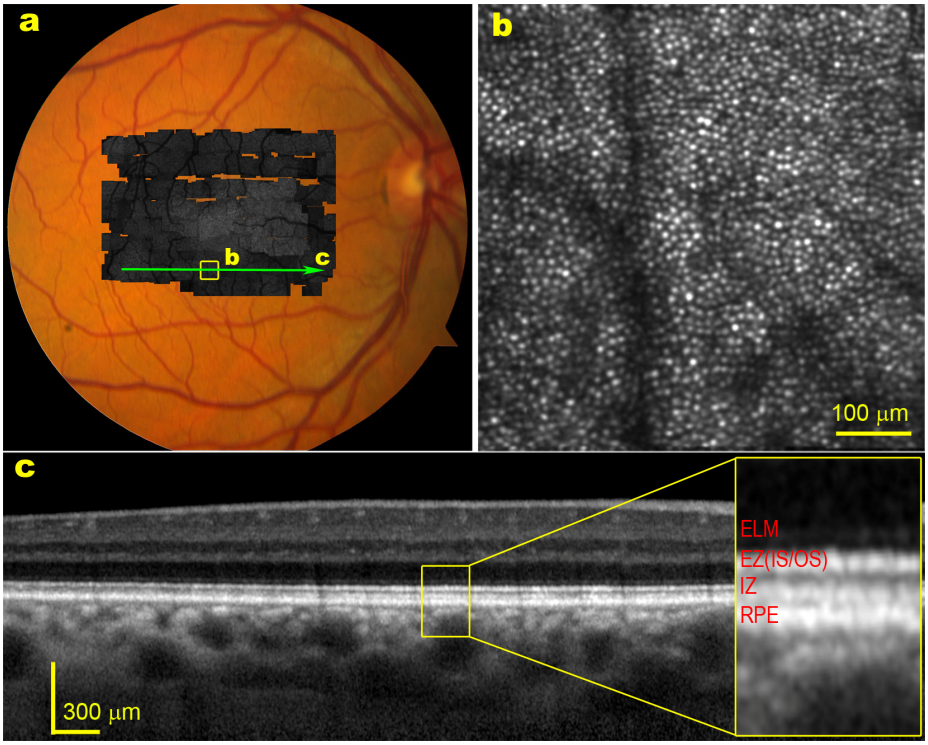

Fig. 1. A healthy retina imaged by AO-SLO and SD-OCT. The subject is a 54-year-old man (white non-Hispanic). (a) The high resolution retinal image montage (gray image) taken with the AO-SLO is overlaid on color fundus photograph. (b) AO-SLO image contained in the box of panel a reveals clear photoreceptor mosaic. The bright spots are cones. The dark bands are the shadow of retinal capillaries. (c) SD-OCT taken through the green arrow-line in panel a.

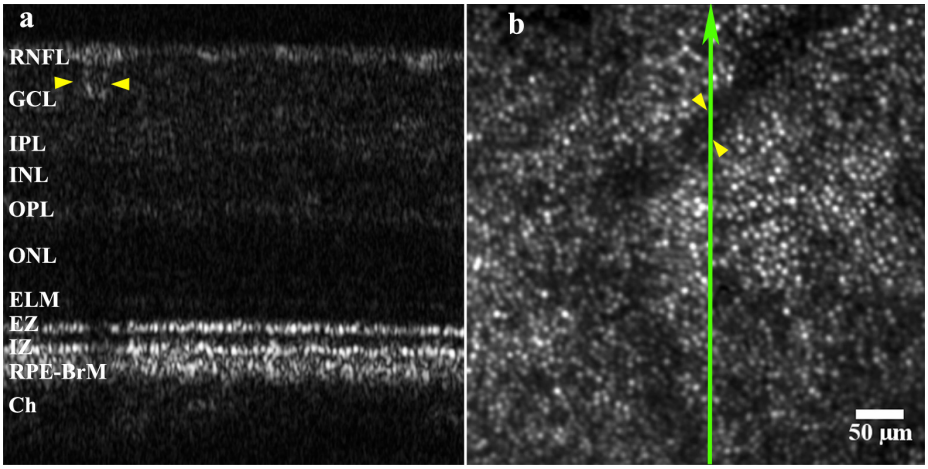

Fig. 2. Healthy retina images. (a) AO-OCT. (b) AO-SLO. The green arrow line on the AO-SLO image shows the approximate scan position of the AO-OCT. The dark band in the AO-SLO image is the shadow of a retinal capillary. The blood vessel and its shadow (indicated by yellow arrowheads) were used as reference landmarks. The bright spots in the AO-SLO images are cone photoreceptors. The retinal layers are marked in the AO-OCT image, RNFL; retinal nerve fibre layer, GCL; ganglion cell layer, IPL; inner plexiform layer, INL; inner nuclear layer, OPL; outer plexiform layer, ONL; outer nuclear layer, ELM; external limiting membrane, EZ; ellipsoid zone, IZ; interdigitation zone; RPE-BrM; retinal pigment epithelium – Bruch's membrane complex. The AO-OCT image is in linear grey scale.

#201230 - $15.00 USD Received 14 Nov 2013; revised 18 Jan 2014; accepted 5 Feb 2014; published 12 Feb 2014

3.2 AO-SLO reveals distinct en face structure of SDD

Multimodal imaging including color fundus photography, confocal IR, RF and AF imaging, as well as SD-OCT provide a comprehensive view and facilitate precise identification of SDD. Figure 3 shows the study case 1, a patient diagnosed with non-neovascular AMD. In a color photograph, SDD appear as an array of yellow-white dots, Fig. 3(a). In an IR image, SDD are revealed with greater prominence, appearing as dark spots, many with a lighter center, Fig. 3(b). In an RF image, SDD appear as an array of light dots, many with a thin darker surrounding ring, Fig. 3(c). In an AF image, SDD appear as an array of spots of decreased autofluorescence, Fig. 3(d). The SD-OCT reveals that SDD are a group of hyperreflective lesions with a triangular shape localizing above (internal to) the RPE layer, Figs. 3(e) and 3(f). The marked SDD have interrupted the EZ(IS/OS) band and extended to the ELM. According to the OCT based SDD grading system [10], these lesions are classified as stage 3. Surrounding the lesion apex is a region of absent OCT signal from the EZ(IS/OS), manifesting as a faint gap on either side of the SDD in this case, as shown in Figs. 3(e) and 3(f). Another notable feature in Fig. 3(e) is that the light has penetrated into the choroid even deeper through the RPE underneath the SDD, forming distinctive light stripes in the choroid.

AO-SLO produced high resolution image of the retina containing these lesions at single cell level, as shown in Fig. 3(g). The retina immediately adjacent to SDD shows a hyporeflective annulus. The most striking feature is the granular texture surrounded by the annulus, which is very similar to the photoreceptors revealed in the surrounding retina. The hyporeflective annulus corresponds to the EZ(IS/OS) gaps on the side of the SDD in the SD-OCT. In this case, the annulus is thin thus the corresponding gap in the EZ(IS/OS) is not distinct. The hyporeflective annuluses may indicate missing, degenerated, or deflected photoreceptors [1, 2].

Figure 4 shows 2 areas in the retina of the study case 2, indicated by the yellow and blue boxes, that were selected for detailed study. In the magnified IR image, SDD appear as a "target" pattern, a reflective core surrounded by an annulus of reduced reflectivity [13]. Again, SDD is shown as hyperreflective material of triangular shape localized in the subretinal space by SD-OCT. The EZ (IS/OS) is not apparent either next to or over the apex of the hyperreflective lesion. These gaps are more apparent than those in Case 1. SD-OCT also shows the distinctive light stripes in the choroid underneath the SDD, indicating increased light throughput and penetration in the region where SDD situate, Figs. 4(e) and 4(f). The AO-SLO renders the distinctive structure of a hyporeflective annulus surrounded reflective core containing photoreceptor-like spots, as shown in Fig. 5(a) and Fig. 6.

To test our impressions that the reflective spots in the speckle texture of the SDD bore a superficial similarity to the reflective spots in the photoreceptor mosaic, we measured the center-to-center spacing of the reflective dots inside and outside the hyporeflective annulus, indicated by red markers in Fig. 6. The measurement shows that the cone spacing at the markers 1 and 2 is 5.3 ± 0.34 μm (mean ± SD), whereas the spacing of the speckle texture of the reflective core (marker 3) is 4.6 ± 0.16 μm, which is significantly smaller ($\alpha = 0.05$, $p<0.001$) than that of the cone spacing. If the speckle pattern were truly attributable to preserved cones, it would be surprising that spacing is smaller (i.e., density is higher) over a lesion. With this initial evidence that reflective material within the stage 3 annulus might not be cones, we investigated it further with additional techniques.

#201230 - $15.00 USD Received 14 Nov 2013; revised 18 Jan 2014; accepted 5 Feb 2014; published 12 Feb 2014

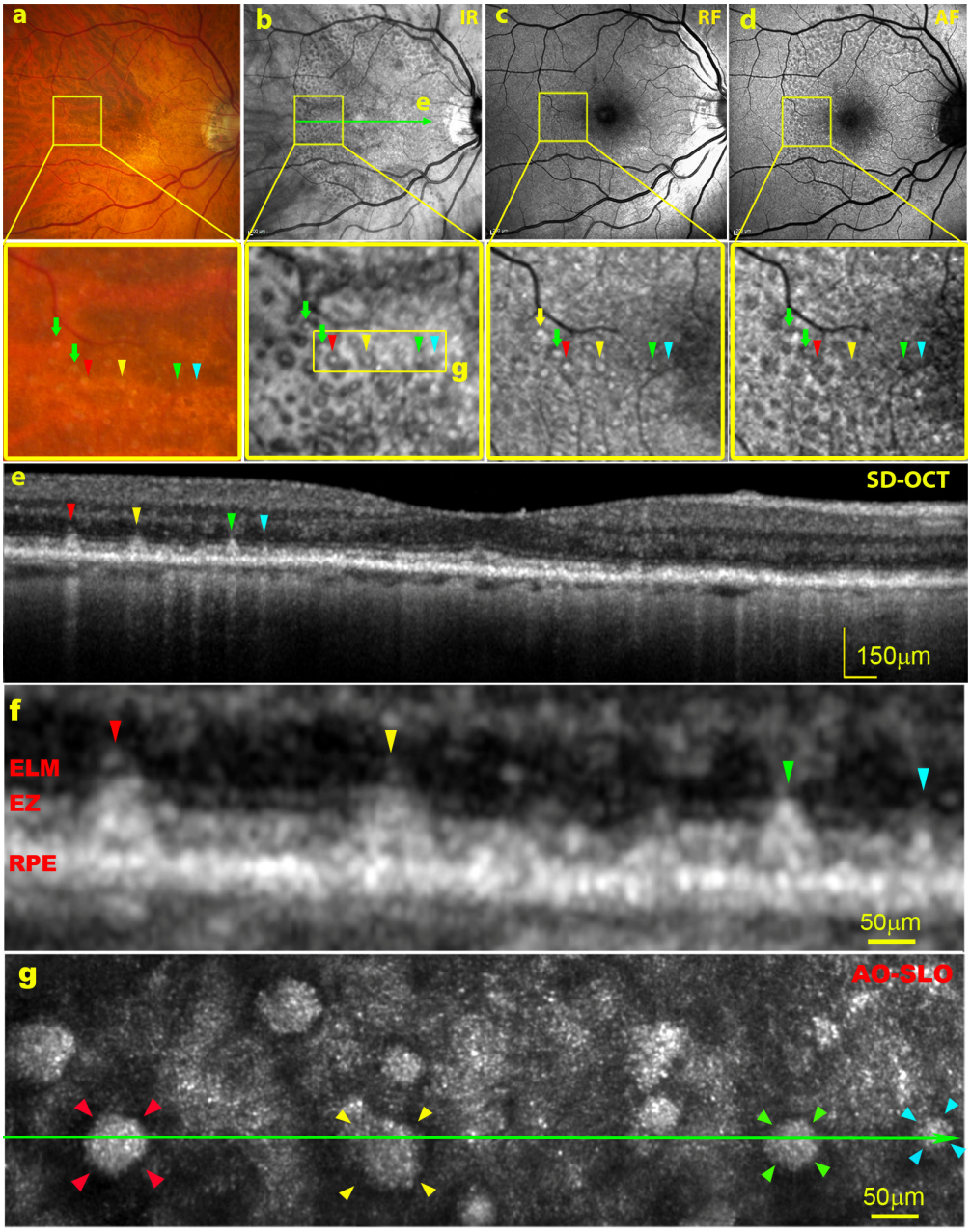

Fig. 3. Multimodal imaging of SDD. The subject (AMD-022) is an 84-year-old woman (white non-Hispanic). AMD severity is graded as 7 (intermediate stage) using the Age-Related Eye Disease Study (AREDS) grading system and the Best Corrected Visual Acuity (BCVA) is 20/20. (a) – (d) are color photograph, IR, RF, and AF images of the macula with a 30 degree field of view, respectively. The retinal areas contained in the boxes in panels (a) – (d) are magnified digitally by 5.4 X. The green arrow-line in panel b indicates where the SD-OCT in panel e was taken. (e) The SD-OCT taken through the line in panel b. Color arrows and arrowheads point to the corresponding SDD rendered with different imaging modalities. These SDD are classified as stage 3. (f) Magnified SDD marked in panel e. (g) The AO-SLO image of the retina indicated by the yellow box in the excision of panel b, revealing the distinctive annular structure of the stage 3 SDD. The reflective spots between the hyporeflective annuluses are photoreceptors. Note the superficial similarity between the reflective texture surrounded by the hyporeflective annulus and the photoreceptors in the area away from SDD.

#201230 - $15.00 USD Received 14 Nov 2013; revised 18 Jan 2014; accepted 5 Feb 2014; published 12 Feb 2014

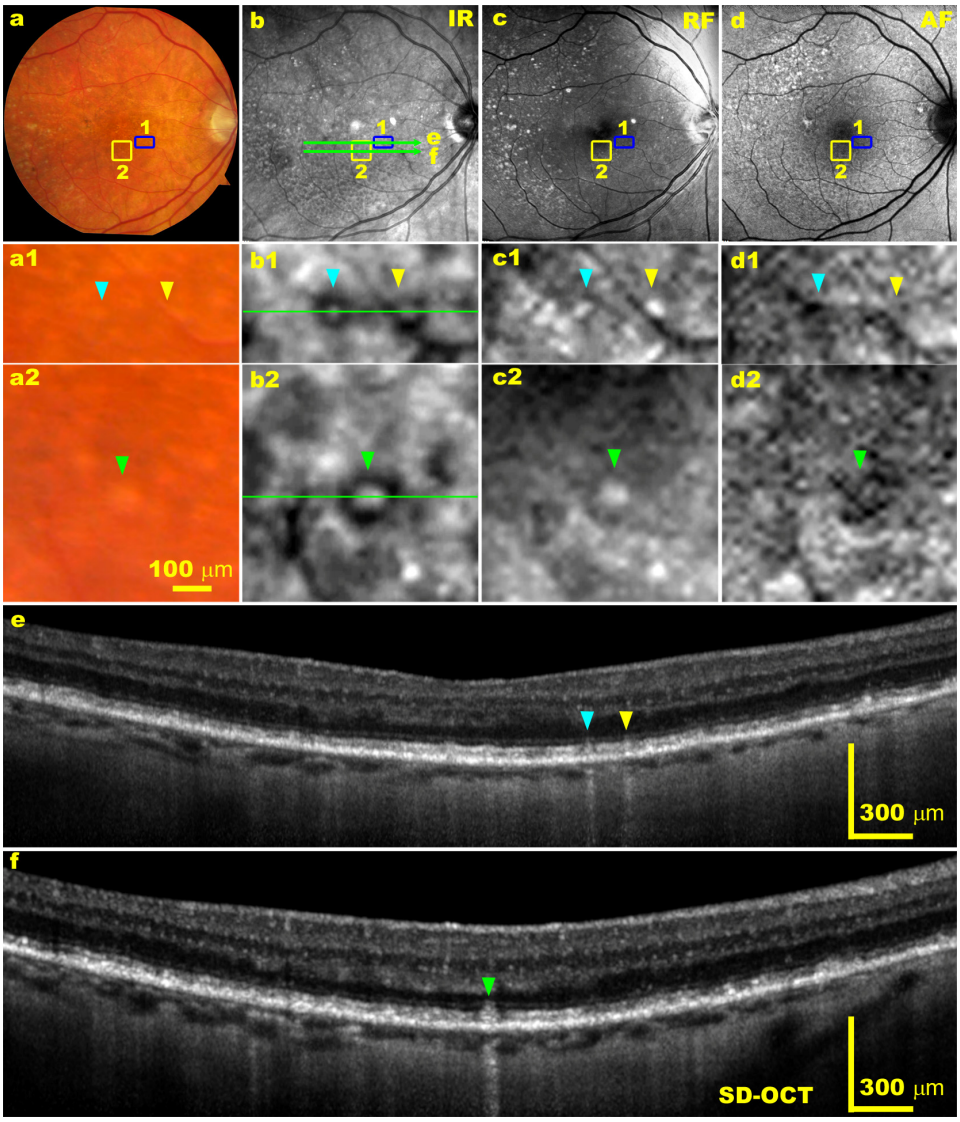

Fig. 4. Multimodal imaging of SDD. The subject (AMD-63) is an 83-year-old man (white non-Hispanic) with non-neovascular AMD. The AREDS grade is 7 and the BCVA is 20/30. (a) - (d) are color photograph, IR, RF, and AF images of the macula with a 30 degree field of view, respectively. (a1) and (a2), (b1) and (b2), (c1) and (c2), (d1) and (d2), are magnification of the areas contained in the blue and yellow boxes in panels a to d, respectively. The green arrow-lines in panel b indicate where the SD-OCT B-scans in panel e and f were taken. (e) and (f) are SD-OCT taken through the lines in panel b. Color arrowheads point to the corresponding SDD imaged in different imaging modalities.

To examine the reflective granular structure surrounded by the hyporeflective annulus, the focus of the AO-SLO was programmed to scan from the top to the bottom of the SDD in a way 'flying focus-though' (Fig. 7, video). The images were continuously recorded. From the supplemental video, we can see that the granular structure are present fairly stable while the focus being moved, indicating that they are real structures inside the lesion. It is also evident that the maximum brightness of the photoreceptors and the granules are not at the same plane, with the photoreceptors brightest at plane internal to the plane in which SDD reflectivity is in focus.

#201230 - $15.00 USD Received 14 Nov 2013; revised 18 Jan 2014; accepted 5 Feb 2014; published 12 Feb 2014

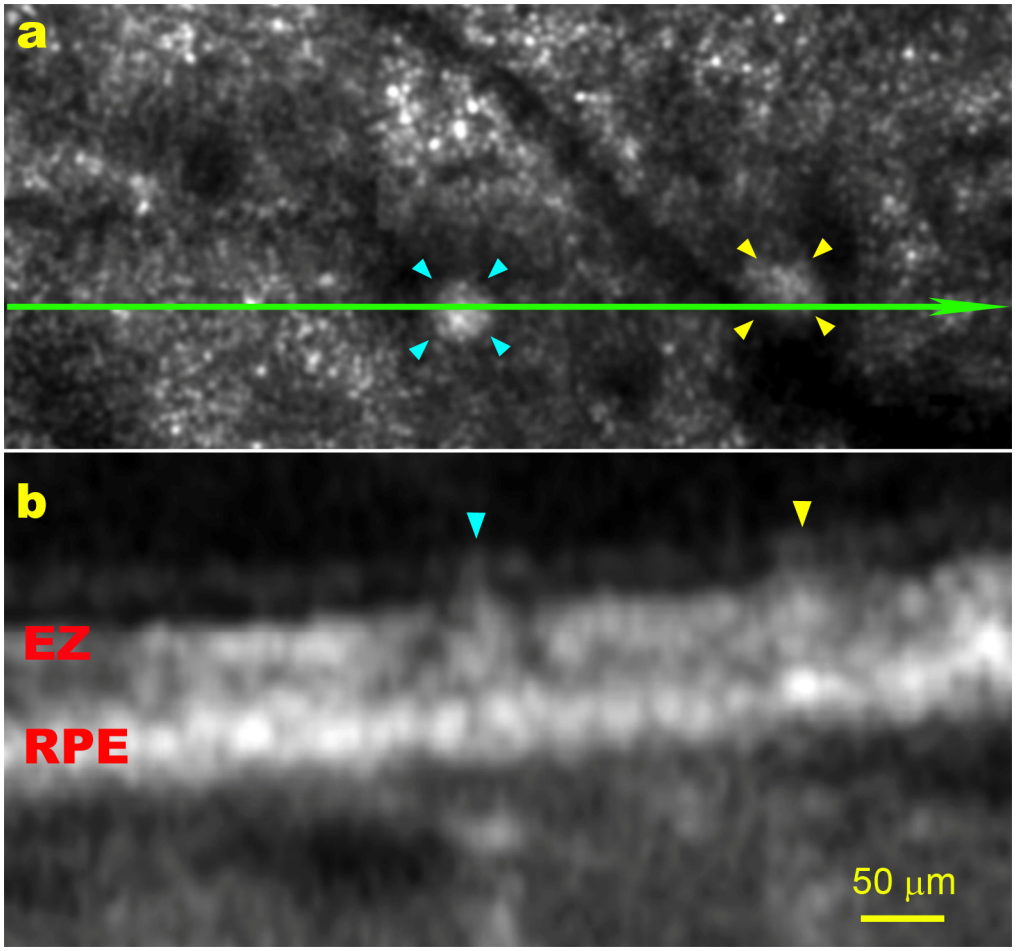

Fig. 5. AO-SLO image of SDD. (a) AO-SLO image of the retina indicated by the blue boxes in Figs. 4(a)-4(d). The reflective spots between the hyporeflective annuluses are photoreceptors. The dark band is the shadow of a retinal capillary. (b) Magnified SD-OCT B-scan of the two SDD in Fig. 4(e). Color arrowheads point to corresponding SDD.

3.3 AO-OCT reveals SDD material

To further understand the microstructure of SDD, high resolution AO-OCT was performed to acquire an image across the SDD studied in Fig. 6. As shown in Fig. 8(a), SDD structure and surrounding retina are rendered with significantly improved lateral resolution compared to the SD-OCT shown in Fig. 8(b). The SDD presents a pile of discrete, hyperreflective granules deposited internal to the RPE, encroaching into the EZ band. There is no discernible EZ above the lesion. It is evident that the speckled texture of the SDD in the AO-SLO image can be attributed solely to the lesion material shown in Fig. 8(a). The AO-OCT also shows that the lesion has little effect on layers of the retina beyond the ELM. Furthermore, the RPE-Bruch's membrane complex appears comparable to that in the normal eye shown in Fig. 1(c).

Figure 9 uses a narrower field to highlight the detail that can be seen with AO enhanced images. The images were taken from the eye of the third study patient. Again, it is apparent that the speckle texture of the SDD in the *en-face* (AO-SLO) plane originates from the SDD material which appears as a pile of granules in the cross-section plane (AO-OCT image).

#201230 - $15.00 USD Received 14 Nov 2013; revised 18 Jan 2014; accepted 5 Feb 2014; published 12 Feb 2014

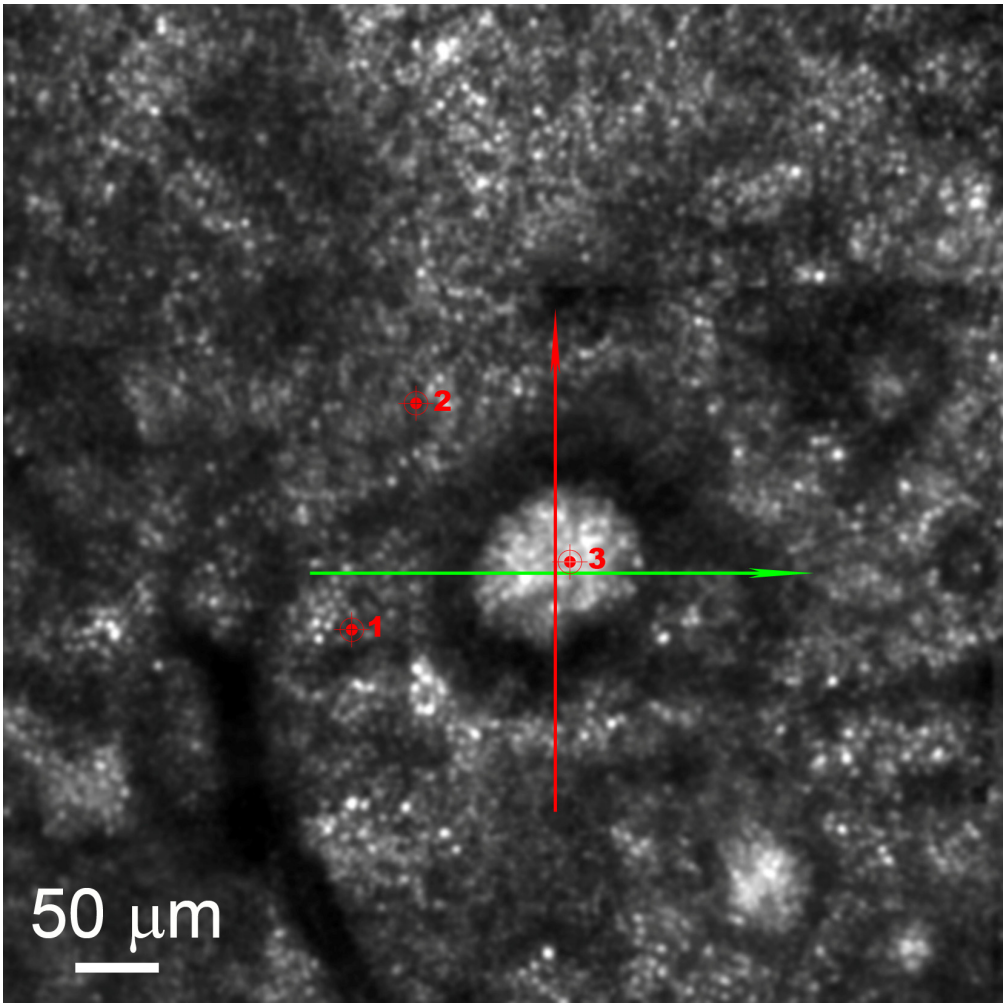

Fig. 6. The AO-SLO image of the retinal area indicated by the yellow boxes in Figs. 4(a)-4(d), a big solitary SDD is imaged. The SDD shows a distinctive hyporeflective annulus surrounding a hyperreflective core. The bright spots outside the hyporeflective annulus are cone photoreceptors. The dark band is the shadow of a retinal capillary. The red arrow line marks where the AO-OCT shown in Fig. 8(a) was taken, whereas the green arrow indicates where the SD-OCT shown in Fig. 8(b) was taken. Red markers with numbers (1, 2, 3) indicate where the center-to-center spacing of the cones surrounding the SDD and the texture of the SDD was assessed

4. Discussion

Our principal finding is *in vivo* microstructure of SDD. In previous studies, *en face* and cross-section structures of SDD were often examined by digitally magnifying a standard colour fundus image or conventional SLO or OCT image [10, 11, 13, 42]. Limited by the pupil size and wavefront aberrations of the human eye's optics, conventional fundus photography, SLO, and OCT can produce retinal images with a lateral resolution of only 10 μm [24, 25]; thus, it is impossible to render the microstructure of the lesion with existing imaging modalities. The significant improvement of the spatial resolution of the AO-SLO-OCT allows investigation of individual lesions at the microscale.

#201230 - $15.00 USD Received 14 Nov 2013; revised 18 Jan 2014; accepted 5 Feb 2014; published 12 Feb 2014

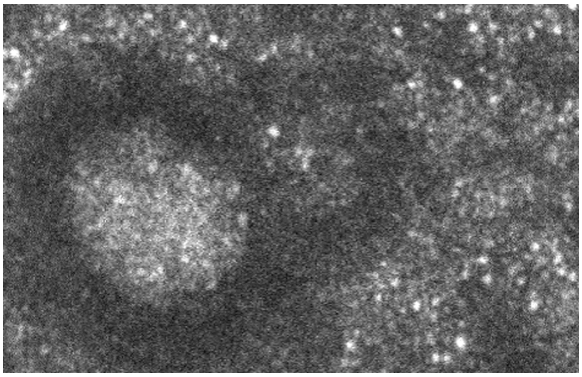

Fig. 7. AO-SLO video of 'flying focus-through' retina (Media 1). The SDD shown in Fig. 6 was imaged. Note that the AO-SLO real time images are vertically flipped compared to the standard funduscopy shown in Figs. 4(a)-4(c) due to scanning optics configuration. The frames have been registered. Image distortion caused by nonlinear scanning of the resonant scanner and by eye movements was eliminated by customized software [36].

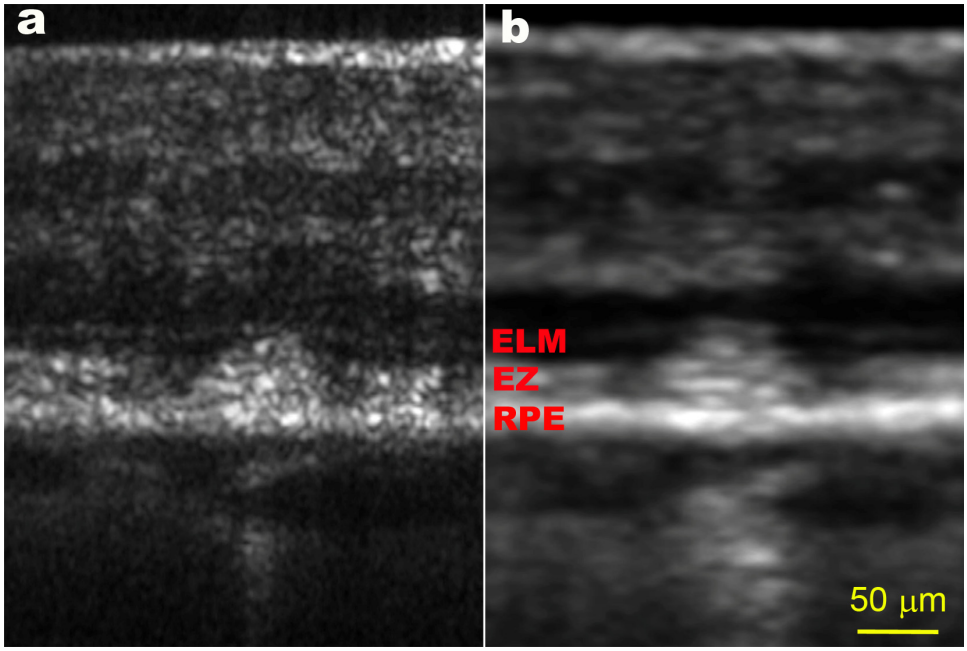

Fig. 8. AO-OCT and SD-OCT of SDD. (a) AO-OCT scanned vertically across the SDD, as indicated by the red arrow line in Fig. 6. The red arrow points to the left side of panel a. (b) SD-OCT B-scan taken along the green arrow-line in Fig. 6. Both images show that this SDD has broken the EZ(IS/OS) band and expanded into the ELM band. The scale bar in panel b applies to both panels. SD-OCT is shown with logarithmic grey scale, whereas AO-OCT scan has a linear grey scale. AO-OCT scan is orthogonal to SD-OCT scan.

AO-SLO revealed a distinct *en face* annular structure of stage 3 SDD. The texture appearing in the reflective core seemingly resembles that generated by the photoreceptors in nearby unaffected retina. AO-SLO has an axial resolution of 50-70 μm [18, 24, 43], about the height of the lesions shown in Figs. 3(e) and 3(f), Fig. 8. This implies that AO-SLO images are essentially formed by the aggregate light reflected from an axial (3D) volume, approximately from the ELM to the apical surface of the RPE. Thus, it is difficult to determine these structures solely by AO-SLO. From the AO-OCT image, it is clear that these structures are formed by light scattered from the lesion material. They may contain

#201230 - $15.00 USD Received 14 Nov 2013; revised 18 Jan 2014; accepted 5 Feb 2014; published 12 Feb 2014

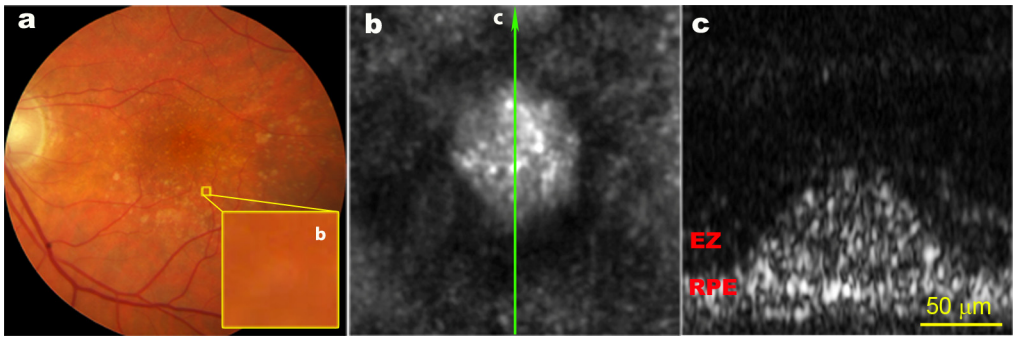

Fig. 9. AO-SLO and AO-OCT imaging of SDD. The subject (AMD-062) is an 81-year-old man (white non-Hispanic) with non-neovascular AMD. The AREDS grade is 6 and the BCVA is 20/20. (a), Digital colour fundus photograph of 30° field of view. The yellow box (b) is with a size of 200 μm (~0.67°) on a side, which is digitally magnified by 15 times, encloses a solitary SDD. (b), The AO-SLO image of the retina contained in the yellow box in panel a, the image is an average of 20 frames. The green arrow line indicates where the AO-OCT scan was taken, pointing to the left side of panel c. (c), AO-OCT image, an average of 10 frames. Panel b and c are with the same scale. The AO-OCT has a linear grey scale.

speckles caused by interference artefacts, especially when the image is taken with high magnification under diffraction-limited conditions. However, similar texture is present in the AO-SLO mode, which uses multiple frame averaging and broadband light that both reduce the amount of speckle in the images [18, 19]. Furthermore, as can be seen from the video of the AO-SLO focusing through the retina depth, while the granules manifest change of reflectivity, they remain with a fairly stable packing structure. This strongly suggests that the speckled texture in both modes arises from the granular nature of the lesions. Higher axial resolution OCT may better confirm whether the texture is caused by interference artefact, real structures, or a mixture of both.

An interesting phenomenon observed in SD-OCT imaging of SDD is the light 'stripes' in the choroid formed by the light penetrating through the RPE underneath the SDD. This indicates a reduction of light absorption in the RPE and may suggest the impact of SDD on the RPE. Direct damage to RPE by SDD might be predicted by the lack of intrinsic cellular anti-oxidant systems to prevent accumulation of toxic molecules in these lesions, and by a hypothesized reduction of capability to phagocytize outer segments of the overlying photoreceptors. However, we have found that not all SDD are associated with these light stripes. It is our hypothesis that these light stripes may be associated with the progression stage of SDD that causes local RPE degeneration. On the other hand, we have also found that the occurrence of light penetration is not associated with the size of SDD. Therefore, it may be possible that the SDD presented in this study may represent a subtype. While the exact reason for this particular phenomenon is unclear, the RPE band underneath the SDD does not manifest alteration or discontinuity with our imaging methods.

The granular texture observed in the AO-OCT images is consistent with histologic descriptions of SDDs, which indicate stereotypic interiors containing a dispersed phase of particulate material containing cholesterol within a flocculent continuous phase that is presumed to be proteinaceous [1, 2]. Important information was learned about conventional drusen in human eye pathology specimens using single-section and quick-freeze deep etch transmission electron microscopy to reveal structure comprehensively and high-resolution light microscopy to reveal selectively stained tissue elements. Specific features of drusen discovered through such studies include the structure of lipoprotein-derived debris [44–46], cores rich in lectin-binding glycoconjugates, unesterified cholesterol, and fibrillar amyloid [47–49], and transitions between hard drusen, which are benign, and soft drusen, which confer high risk [50]. In concert with our planned laboratory studies, visualization of SDD fine structure in living patients through AO-SLO-OCT can accelerate understanding of how

#201230 - $15.00 USD Received 14 Nov 2013; revised 18 Jan 2014; accepted 5 Feb 2014; published 12 Feb 2014

these lesions contribute to progression towards AMD end-stages and what they signify about under-explored aspects of outer retinal physiology [9], as specified in the 2-lesion, 2-compartment hypothesis of AMD lesion biogenesis [2].

There are limitations to this study. AO-OCT can scan in only one direction, so volumetric imaging of SDD is not achieved. Older subjects tend to have poor fixation leading to fast and random retinal movement, making it extremely difficult to achieve 3D volumetric scan in a small field of view. The variety of SDD appearances in clinical imaging and histology are suggestive of multiple subtypes that are yet to be defined and are not fully captured by our study. Of these subtypes, we imaged only the structure of solitary (non-confluent) SDD. In future studies, by selecting subjects with clearer optical media and developing new software, the extent of photoreceptor perturbation will be examined quantitatively and longitudinally on a per lesion basis. Despite these limitations, the high resolution *en face* and cross-sectional images of the retina produced by the AO-SLO-OCT have greatly improved our understanding of the microstructure of SDD in AMD patients.

5. Conclusion

Because of their proximity to the overlying photoreceptors, SDD may impose a more direct impact on the optical properties and structure of these cells. Thus, direct and precise assessment of the structure of SDD, and more importantly, the impact of SDD on surrounding photoreceptors, is critical to our understanding of disease pathophysiology and thus to the development of effective treatments. The AO-SLO-OCT may be an effective tool facilitating this task.

Acknowledgments

This project is funded by EyeSight Foundation of Alabama (YZ), International Retina Research Foundation (YZ), 5R21EY021903 (YZ), Songs for Sight, Buck Trust of Alabama, R01EY06109 (CC), and institutional support from Research to Prevent Blindness, EyeSight Foundation of Alabama, Buck Trust of Alabama, and NIH P30 EY003039. The authors gratefully thank the Clinical Research Unit of UAB Department of Ophthalmology led by Dr. Cynthia Owsley for assistance of study patients recruitment and standard ophthalmoscopy. The authors also thank Qiang Yang, PhD, Montana State University, for helping develop the AO-SLO image process software. AO-OCT images were registered using the StackReg plugin provided by http://bigwww.epfl.ch/thevenaz/stackreg/#LegalBlurb.